Calculation of point defects in rutile TiO_2 by the screened-exchange hybrid functional

Hsin-Yi Lee (李欣怡),[1] Stewart J. Clark,[2] and John Robertson[1,*]
[1]*Engineering Department, Cambridge University, Cambridge, CB2 1PZ, United Kingdom*
[2]*Physics Department, Durham University, Durham, DH1 3LE, United Kingdom*
(Received 29 June 2012; revised manuscript received 1 August 2012; published 31 August 2012)

The formation energies of the oxygen vacancy and titanium interstitial in rutile TiO_2 were calculated by the screened-exchange (sX) hybrid density functional method, which gives a band gap of 3.1 eV, close to the experimental value. The oxygen vacancy gives rise to a gap state lying 0.7 eV below the conduction band edge, whose charge density is localized around the two of three Ti atoms next to the vacancy. The Ti interstitial (Ti_{int}) generates four defect states in the gap, whose unpaired electrons lie on the interstitial and the adjacent Ti 3*d* orbitals. The formation energy for the neutral oxygen vacancy is 1.9 eV for the O-poor chemical potential. The neutral Ti interstitial has a lower formation energy than the O vacancy under O-poor conditions. This indicates that both the O vacancy and Ti_{int} are relevant for oxygen deficiency in rutile TiO_2 but the O vacancy will dominate under O-rich conditions. This resolves questions about defect localization and defect predominance in the literature.

DOI: 10.1103/PhysRevB.86.075209 PACS number(s): 71.20.Nr, 71.15.Mb, 73.20.At, 82.65.+r

I. INTRODUCTION

Titanium dioxide (TiO_2) is a transition metal oxide with a closed shell electronic structure and a band gap of 3.05 eV. It is an important material for photocatalysis, solar cells, and environmental cleanup, due to unusual photocatalyic behavior.[1–4] Oxygen deficiency defects such as surface oxygen vacancies are held to be critical for such applications. TiO_2 is also interesting in electronics. It has a high dielectric constant but its band offset is too low for it to be useful as a high dielectric constant gate dielectric.[5] On the other hand, it is of considerable interest for use in nonvolatile resistive random access memories (RRAM).[6,7] The conductive track in the on-state is believed to arise from a percolation path of oxygen vacancies or similar defect across the film. Thus, the behavior of excess electrons and associated defects is critical to the performance of TiO_2 as a catalyst or in electronics.

It is known from ultraviolet photoemission spectroscopy (UPS) and electron energy loss spectroscopy (EELS) that the oxygen deficiency defects give rise to gap states lying about 0.7 to 1.0 eV below the conduction band edge.[8–13] However, the origin and localization of these states are still contentious. Electron spin resonance (ESR) showed that unpaired electrons associated with the oxygen vacancy are localized on two of the three Ti sites adjacent to the vacancy.[14] For many years, catalytic activity has been discussed in terms of surface oxygen vacancies, based on resonant photoemission or EELS. However recently, Wendt *et al.*[15] interpreted scanning tunneling microscopy (STM) maps in terms of a dominant role of Ti interstitials. Mass transport during TiO_2 growth also suggested that Ti interstitials were involved.[16,17] This debate has continued, with recently resonant photoemission spectra again suggesting that localized gap states were due to the oxygen vacancy.[18–20]

Electronic structure calculations of these defects should be able to define the dominant defect and say how localized their defect states are. There have been many calculations of the defects of TiO_2 using the local density approximation (LDA) or generalized gradient approximation (GGA).[21–25] However, LDA and GGA are known to underestimate band gaps, and give defect states that are too delocalized because of a lack of self-interaction cancellation.[26,27] This failure is very important for a material like TiO_2 where the defect states are on the borderline between shallow and deep, and where the degree of localization is the key question.

One method to correct these problems is the LDA + U method, in which an on-site repulsion U is added to the transition metal d states.[28–43] This can widen the band gap of TiO_2 slightly, but LDA + U is best used for open shell systems. On the other hand, LDA + U does give a better description of defect localization, and it has been widely used for bulk and surface defects.[29–43] Morgan and Watson[30] found that $U \sim 5$ eV gives a reasonable description of defect localization even if the band gap is still underestimated compared to the experimental value of 3.05 eV.[44]

Pacchioni[27] and Sauer *et al.*[28] have discussed the need for the correct description of defects in the catalysis problem, and the problems with various electronic structure methods. The defect localization in TiO_2 comes not only from the electronic state, but also the interaction of electronic states with lattice distortions—a polaronic effect, as noted generally by Lany and Zunger.[45] Hybrid density functionals are a better method to tackle such cases, because they combine a much improved description of the exchange energy and, as generalized Kohn-Sham functionals, they can be used for total energy minimization and structure relaxation. Di Valentin *et al.*[46–48] used the hybrid functional B3LYP to describe electron excess defects in TiO_2 and compare the results to LDA + U. This work provided a good understanding of the general defect properties, where the subtle energy differences between localized and delocalized defect states became apparent. Their results required some interpretation because their B3LYP overestimated the TiO_2 band gap at 3.9 eV. In contrast, Muscat *et al.*[49] found a gap of 3.4 eV in their B3LYP results. Zhang *et al.*[50] noted that including 13% Hartree-Fock exchange can give the correct band gap of rutile TiO_2.

Janotti *et al.*[51] and Deak[52] have employed the widely used hybrid function HSE06 functional[53,54] to study the electronic properties of the oxygen vacancy and substitutional dopants.

 ©2012 American Physical Society

Janotti[51] found that HSE gave a greatly improved description than GGA, but they did not treat the Ti interstitial. They found the vacancy to have localized states in the gap but that the transition level was shallow.

A further improvement on the various methods might be possible using the GW method, but this would lose the simplicity of a single shot approach to structural relaxation for polaronic defects. We therefore employ here the screened-exchange (sX) hybrid density functional[55–58] to treat the vacancy and interstitial defects. The sX method has been found to give the correct band gaps of a wide range of semiconductors such as the III-Vs, ZnO and SnO_2, and the insulators HfO_2 and SiO_2,[57] and the correct localization of holes in the Al doped SiO_2 (smoky quartz)[59] and at the Zn vacancy in ZnO.[60] It also describes correctly the correlated systems such as the transition metal oxides Ti_2O_3, Cr_2O_3, Fe_2O_3,[61] and the lanthanide oxides Ln_2O_3[62] and NiO, FeO, and MnO.[61] Its better description of the lanthanide oxides than HSE arises from its slightly better treatment of the highly localized $4f$ states, and this might be valuable in the present case where defects are on the shallow-deep border line.

II. METHODS

The sX method is a hybrid density functional which replaces part of the short-range part of exchange in LDA with a Thomas-Fermi screened nonlocal exchange as in Hartree-Fock. It can therefore be self-interaction free. The exchange term is constructed to satisfy both the low-electron density and the free-electron gas limits. The screened-exchange potential is expressed as

$$V_{\rm sX}(r,r') = -\sum_i \frac{\psi_i(r)e^{-k_{\rm TF}|r-r'|}\psi_j^*(r)}{|r-r'|}, \tag{1}$$

where i and j label the electronic bands. The $k_{\rm TF}$ is a Thomas-Fermi screening length. This can be set to the average valence electron density of the system, or given by a fixed value. Here we set $k_{\rm TF}$ to 2.15 Å^{-1} by considering the experimental value of the band gap of rutile TiO_2. sX belongs to a class of generalized Kohn-Sham functionals so it can be used variationally for energy minimization, using the calculation of forces.[56]

The calculations were performed with the CASTEP plane wave pseudopotential code.[63] The cores were represented by norm-conserving pseudopotentials, while the valence states were expanded in a plane-wave basis set with 750 eV cutoff energy. For k-space sampling we used the Γ point in defect supercells. The geometry optimization used the Broyden-Fletcher-Goldfarb-Shannon (BFGS) algorithm with convergence to 5×10^{-5} eV per atom, 0.1 eV/Å for the Hellmann-Feynman force on each atom, and a stress of 0.2 GPa.

The defect calculations use $2 \times 2 \times 3$ supercells of 72 atoms plus the defect. A series of convergence tests had been applied to determine the computational parameters, including the cutoff energy, k point, and supercell size. Because of the polaronic nature of the defect, the defect supercell was relaxed in sX to obtain the correct lower symmetry geometry. A larger supercell of $3 \times 3 \times 4$ units (216 atoms) was calculated to check the finite-size effects. We found the formation energy changed by less than 0.25 eV going from 72 to 216 atoms, and the transition levels changed by less than 0.11 eV. The results obtained from the Γ point and two special k points (0, 0, 0) and (0.25, 0.25, 0.25) are also quite similar, with only a 0.16 eV difference. Thus, we think the sX calculations on a $2 \times 2 \times 3$ supercell with a Γ point are adequate, as used by others.[51]

We used spin polarization for the odd charge states to describe the unpaired electrons; for even charge cases, we have checked the results with and without spin polarization, and the data show negligible difference. For comparison, we also carried out the GGA-PBE calculations for the band gap which implied the ultrasoft pseudopotential with 380 eV cutoff energy in $5 \times 5 \times 8$ k-point mesh, to treat as a reference to compare with the sX results.

For the calculation of defect formation energy in the different charge states, the overall supercell size was kept fixed at the relaxed neutral bulk value. The defect formation energy (H_q) of charge q as a function of the Fermi energy (E_F) and the chemical potential $\Delta\mu$ of element α is given by[64]

$$H_q(E_F,\mu) = [E_q - E_H] + q(E_V + \Delta E_F) + \sum_\alpha n_\alpha(\mu_\alpha^0 + \Delta\mu_\alpha), \tag{2}$$

where E_q and E_H are the total energy of a defect cell and a perfect cell, respectively, calculated of charge q, ΔE_F is the Fermi energy with respect to the valence band edge, n_α is the number of atoms of element α, and $\mu^0{}_\alpha$ is reference chemical potential, following the method described by Lany and Zunger.[64]

III. RESULTS

A. Bulk

There are three polymorphs of TiO_2, rutile, anatase, and brookite. Here we study the most common phase rutile. TiO_2 rutile has a six-atom tetragonal unit cell with the $P4_2/mnm$ space group. This lattice consists of threefold coordinated oxygen atoms and octahedral Ti atoms (Fig. 1). The defect configurations are shown in Fig. 2.

The band structures of TiO_2 derived from the GGA-PBE and the sX are shown in Figs. 3(a) and 3(b), respectively. Table I compares the lattice constants, band gaps, and valence bandwidths from the GGA-PBE, sX, and the experimental data.[44,65,66] We found that the band gap increases from 1.86 eV in GGA-PBE to 3.1 eV in sX, very close to the experimental value of 3.05 eV. The valence bandwidth increase from

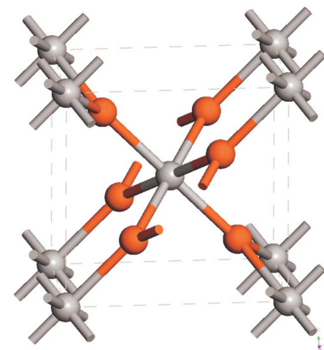

FIG. 1. (Color online) A unit cell of rutile TiO_2 where the red spheres represent O atoms and the gray spheres represent Ti atoms.

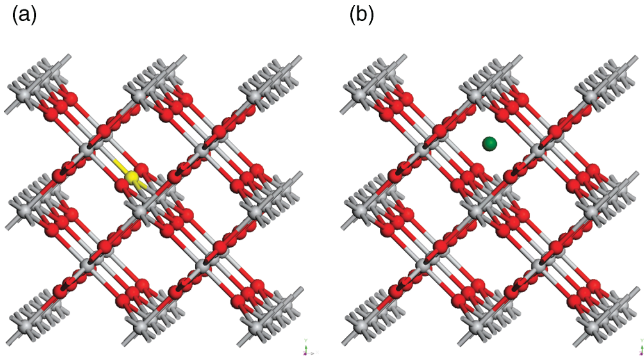

FIG. 2. (Color online) The crystal structures for rutile TiO_2 of (a) O vacancy and (b) Ti interstitial. O vacancy is represented by a yellow ball, Ti interstitial is represented by a green ball.

5.65 eV in PBE to 6.27 eV in sX, which is closer to the experimental value of 6.0 eV.[65] The heat of formation changes from −9.33 eV in PBE to −9.73 eV in sX, the latter is very close to the experimental value of −9.74 eV. The a lattice constant changes from 4.65 Å in PBE to 4.56 Å in sX, which is now slightly below the experimental value of 4.59 Å.

B. Oxygen vacancy

We first consider the oxygen vacancy. Figure 4 shows the plan view of ion-ion spacings around the ideal vacancy, without

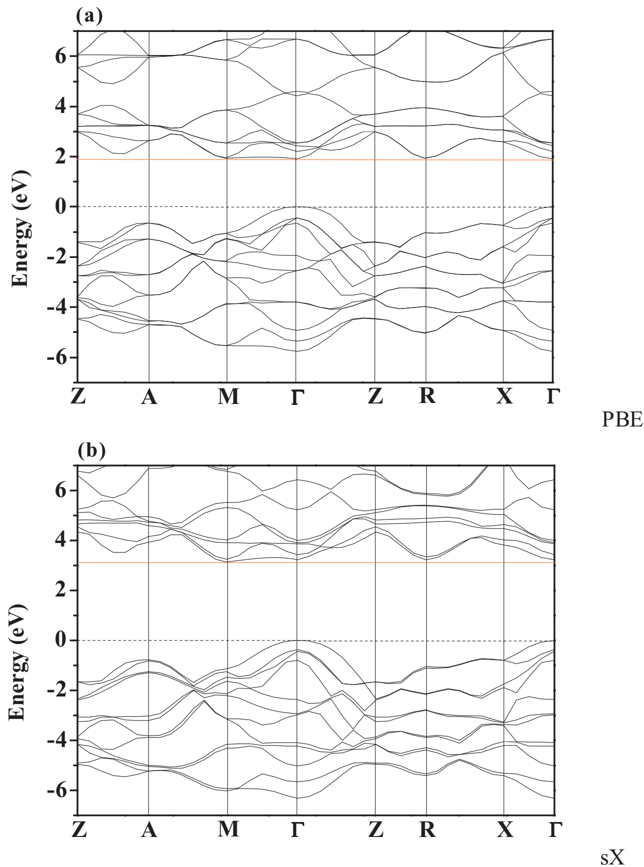

FIG. 3. (Color online) Band structures of rutile TiO_2 calculated by (a) the GGA-PBE and (b) the sX methods. The horizontal red line marks the minimum of the conduction band.

TABLE I. Lattice parameters, heat of formation, minimum band gaps, and valence bandwidths of rutile TiO_2 from GGA-PBE, the sX method and experiment.[44,65,66]

	PBE	sX	Experiment
Lattice constant, a (Å)	4.65	4.56	4.59
c/a	0.639	0.648	0.644
u	0.305	0.305	
Heat of formation ΔH_f (eV)	− 9.33	− 9.73	− 9.74
Band gap (eV)	1.86	3.1	3.05
VB width (eV)	5.65	6.27	6

relaxation. Removing one oxygen atom from TiO_2 results in two unpaired electrons and three Ti dangling bonds. The ideal spacings between adjacent Ti atoms are two at 3.55 Å and one along the c axis at 2.99 Å. We denote V_O^0, V_O^+, and V_O^{2+} for the neutral, singly charged, and doubly charged states, respectively, for the oxygen vacancy. For V_O^0, after relaxation the adjacent Ti atoms move outwards, so the Ti-Ti distance increases to 3.7 Å, and 3.04 Å along the c axis. For the singly positive vacancy V_O^+, the positive charge causes a greater repulsion for a Ti-Ti distance to 3.85 Å and 3.12 Å along Oz. For V_O^{2+} the Ti-Ti distance increases to 3.94 Å and 3.22 Å along Oz. In other words, the lattice relaxation is 4.2% for V_O^0, 8.5% for V_O^+, and 11% for V_O^{2+}. A similar outward relaxation is found for the O vacancies in other ionic oxides such as HfO_2 and ZnO.[58,67]

The defect formation energies can be calculated as a function of O chemical potential. The chemical potentials satisfy $\mu_{Ti} + 2\mu_O = H_f(TiO_2) = -9.73$ eV (experimental value). The O rich limit is $\mu_O = 0$ eV and $\mu_{Ti} = -9.73$ eV, corresponding to the chemical potential of the O_2 molecule. The Ti-rich limit corresponds to the equilibrium of TiO_2 and Ti_2O_3 (not TiO_2/metallic Ti as in many cases) or $\mu_O = -4.07$ eV, $\mu_{Ti} = -1.59$ eV. The metallic Ti/TiO_2 equilibrium would correspond to $\mu_O = -4.86$ eV and $\mu_{Ti} = 0$ eV.

Figure 5 shows the calculated formation energies of the oxygen vacancy and Ti interstitial of rutile TiO_2 for both O-poor and O-rich conditions in sX. For V_O^0 in the O-rich condition, the calculated formation energy is +5.7 eV, corresponding to +1.9 eV for the O-poor condition. The transition energy levels correspond to the Fermi energy where the charge q and q' defect states have the same formation energies. The calculated transition energy of V_O^0/V_O^{2+} in sX is ∼0.7 eV below the conduction band minimum E_C. Thus, the O vacancy is a deep defect. We see that the different charge states of the O vacancy all cross at 0.7 below E_C, so that the effective correlation energy U of this defect is about 0. Similarly, U for the Ti interstitial is close to 0 in our sX results. Nevertheless, this does not stop the paramagnetic states of these defects being observed.

Figure 6 shows the partial density of states (DOS) of the defect sites for the three charge states V^0, V^+, and V^{2+}. In sX the oxygen vacancy gives rise to a defect state lying well inside the band gap, as been found in the DOS for V_O^0 and V_O^+. The energy of the gap state is around 0.7 eV below the conduction band edge, and agrees well with the experiments.[8] For the V_O^0 the defect state is occupied by two electrons; for the V_O^+ it is occupied by one electron. There is no gap state

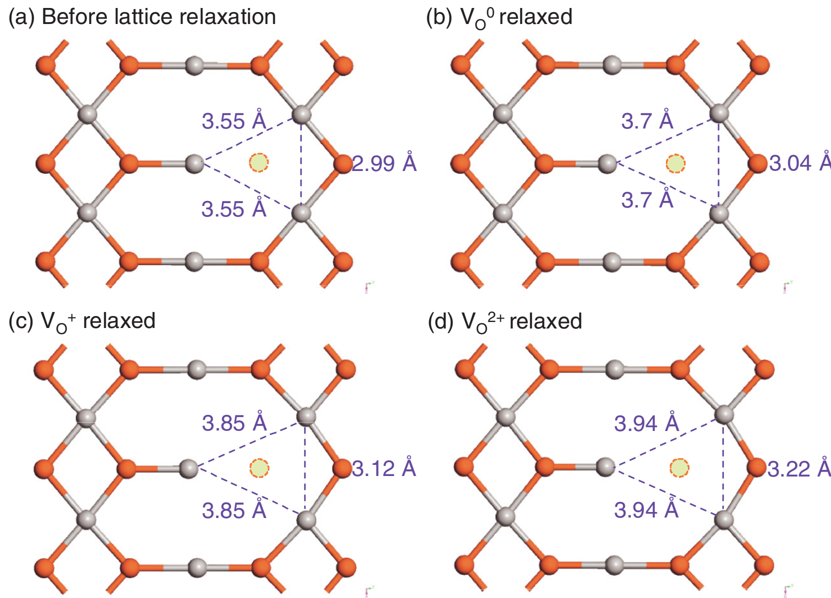

FIG. 4. (Color online) Plane view of ion-ion spacings around the O vacancy site (yellow circle) after the geometry optimization carried out by the sX functional: (a) Before lattice relaxation, (b) $V_O{}^0$ relaxed, (c) $V_O{}^+$ relaxed, and (d) $V_O{}^{2+}$ relaxed.

for $V_O{}^{2+}$ because the excess electrons at the vacancy site have been ionized.

Figure 7 shows the charge density map of the defect state for $V_O{}^0$ and $V_O{}^+$. The neutral vacancy is $S = 1$ with the electrons localized on two of the three adjacent Ti atoms next to the vacancy along the Oz axis, rather than on the vacancy itself. In the positive vacancy the unpaired electron is also in a gap state mainly localized on the two adjacent Ti atoms along the Oz axis. Both these are consistent with the EPR data.[14]

We found that the localization can also depend on the Ti pseudopotential. We also used Ti pseudopotential generated by the OPIUM method[68] to study the oxygen vacancy defect in rutile TiO_2. Except for the pseudopotential, all other settings such as k_{TF} were the same. The resulting DOS also has a defect state in the gap, but the state for $V_O{}^0$ is localized on the d_{xy} orbital, which is contrary to experimental findings. This shows the subtle effects that can occur in this borderline deep state, although we did not carry out a systematic study of many potentials. We have also varied k_{TF} for fixed potentials and looked at the variation of band gaps.

C. Titanium interstitial

Ti interstitial is the other key defect in reduced titania. It occupies an octahedral site surrounded by six O atoms [Fig. 2(b)]. The Ti interstitial has charge states $Ti_i{}^0$ to $Ti_i{}^{4+}$. After atomic

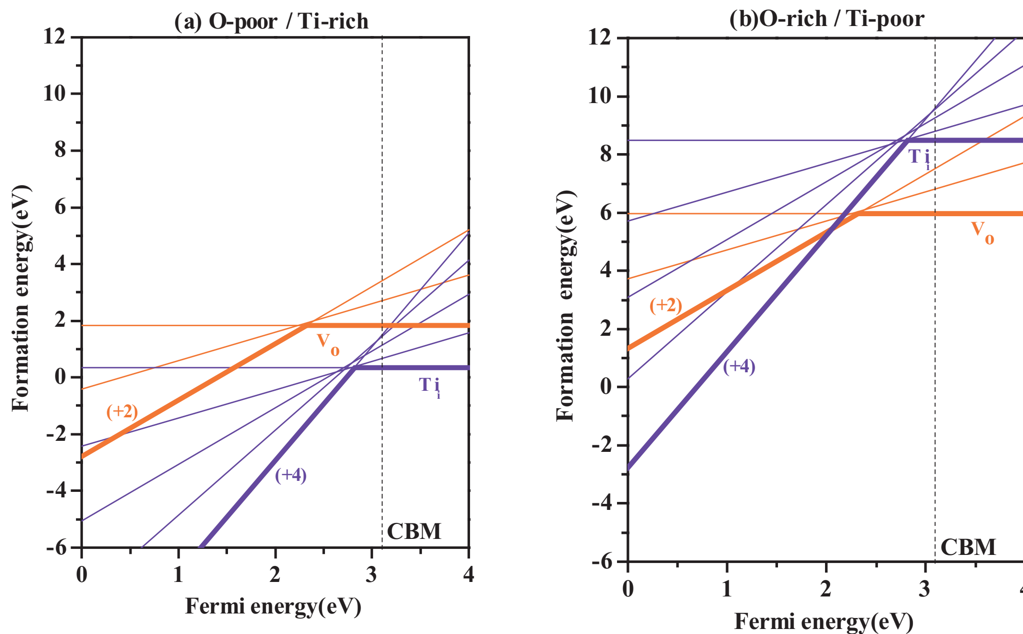

FIG. 5. (Color online) The defect formation energy against Fermi level of the O vacancy (red lines) and Ti interstitial (blue lines) under (a) O-poor and (b) O-rich conditions, calculated by the sX functional for rutile TiO_2. The vertical dash lines denote the conduction band minimum (CBM). The slope of the formation energy lines gives the charge state of the defect.

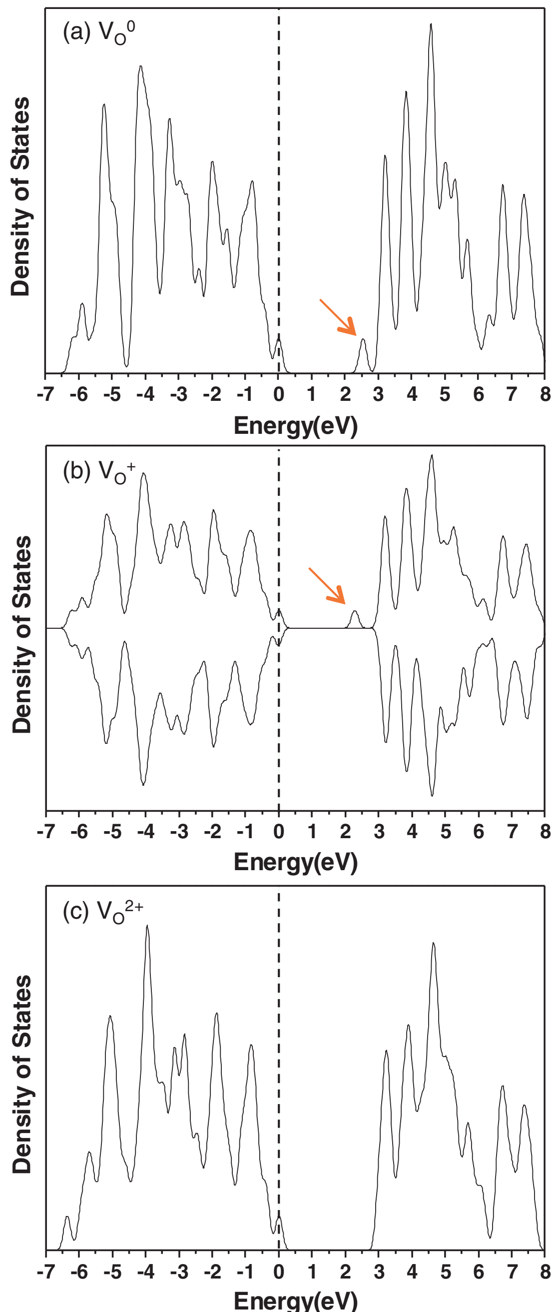

FIG. 6. (Color online) The density of states (DOS) of rutile TiO_2 in the sX method: (a) $V_O{}^0$, (b) $V_O{}^+$, and (c) $V_O{}^{2+}$. The arrows indicate the defect states within the band gaps. For $V_O{}^+$ the spin-up and spin-down states are shown, respectively, above and below the abscissa. The top of the valence band is set to be the zero energy and is denoted by the vertical dash line.

relaxation by the sX functional for the neutral charge state ($Ti_i{}^0$), we found the inserted Ti atom pushes away the adjacent O atoms, forming a longer bond length at the octahedral site, as in Fig. 8. The relaxed Ti-Ti distance is 2.59 Å, while the original distance is 2.28 Å. There are two different Ti-O lengths in the lattice, one is from 1.65 Å and expands to 1.99 Å, the other is from 2.23 Å and slightly shortens to 2.02 Å.

Figure 9 shows the density of state of $Ti_i{}^0$ in rutile TiO_2. It is worth mentioning that spin polarization is necessary to accurately describe the defect states of the Ti interstitial. We performed the nonspin polarized sX computation and found that only two peaks appeared near the conduction band minimum for $Ti_i{}^0$. We then applied the spin polarization, and the DOS now shows four defect states lying in the band gap at 0.7–1.3 eV below the conduction band edge, which is consistent with the experimental data.[8–12] Thus, sX also gives the Ti_{int} as a deep state. From the charge density contours of the defect states in Fig. 10, we found that the trapped electrons of the Ti interstitial were fully localized on the Ti 3*d* orbitals at the inserted and adjacent Ti atoms. It supports the observation that the Ti^{3+} ion is formed by Ti interstitial. Finazzi *et al.*[69] also noted the need for spin-polarized calculation for Ti interstitial in their B3LYP calculations. Their nonspin-polarized B3LYP calculations on $Ti_i{}^0$ obtained only a doubly occupied state with higher total energy that does not account for the EPR data.[69,70]

These calculations will be extended to other donor systems such as interstitial hydrogen, which forms a localized but relatively shallow donor state in TiO_2.[47,71,72]

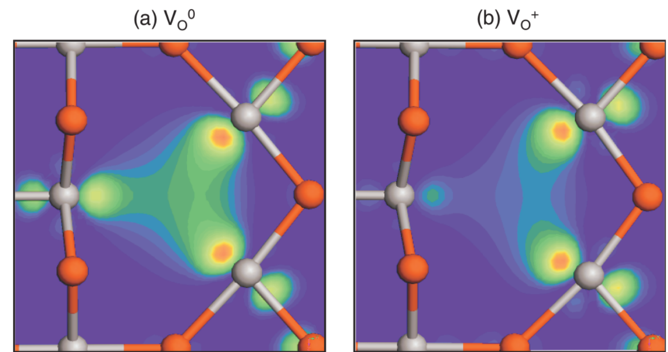

FIG. 7. (Color online) Charge density contour for the oxygen vacancy site of rutile TiO_2: (a) $V_O{}^0$ and (b) $V_O{}^+$, calculated by the sX functional.

D. Discussion

We compare our results for these two defects with those of others, following Table II. Janotti *et al.*[51] calculated the O vacancy with the closely related HSE functional. They found very similar bulk thermodynamic and structural properties to our values for sX. Their formation energy for the neutral oxygen vacancy in Ti-rich conditions of 1.8 eV is also very close to us. It is interesting that the formation energy value

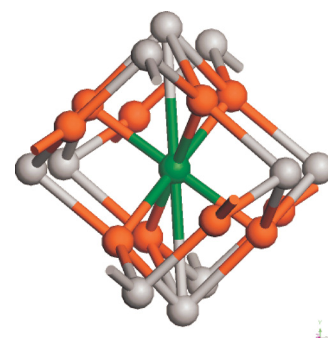

FIG. 8. (Color online) Equilibrium geometry of $Ti_i{}^0$ in rutile TiO_2 calculated by sX. Ti interstitial is shown green.

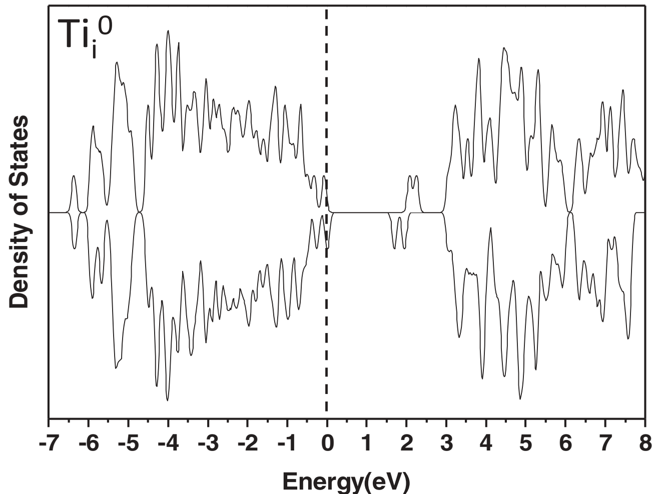

FIG. 9. The density of states (DOS) of $Ti_i{}^0$ in rutile TiO_2 calculated by the sX method.

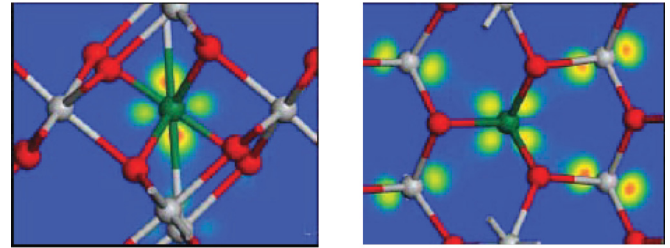

FIG. 10. (Color online) The charge density contours of the four in-gap defect states of the neutral Ti interstitial, calculated by the sX functional. (a) and (b) are (010) and (110) plane, respectively. The interstitial Ti atom is shown as a green sphere.

for $V_O{}^0$ is within ± 0.1 eV for both hybrid functionals sX and HSE. However, they found a slightly lower formation energy for V_O^{2+} so that they found the $0/2+$ transition level of V_O to occur at the conduction band edge, as a shallow donor, whereas sX finds the $0/2+$ transition level to be 0.7 eV deep in our sX results. The sX result is consistent with EELS experiments[12] and also the localization of the defect wave function in ESR.[14] The difference is likely to arise from a small difference in the Ti pseudopotential or the exchange screening of sX compared to HSE. From our convergence tests it is less likely to arise from supercell size effects; these tend to move formation energies up or down, but affect the transition levels less. Note that Janotti *et al.*[51] did not study the interstitial, the only comparable calculations use B3LYP.

The B3LYP calculations of DiValentin *et al.*[47] found similar defect wave function localizations as us, but their band gaps were higher than us, so the defect levels appear deeper in the gap. They did not plot their defect properties as formation energies.

Interestingly, the early calculation of Zhang *et al.*,[50] who varied the fraction of HF exchange to fit the bulk band gap, got much of the defect localization correct.

There have been numerous defect calculations using GGA + U. We focus on those that gave formation energy data as a function of Fermi energy.[33,36] We first note that this method usually underestimates the band gap for the U parameters chosen. It also gives less accurate values for the bulk heat of formation than HSE or sX.

Morgan and Watson[33] studied the oxygen vacancy formation energy using the GGA + U approach. They found a formation energy for the neutral O vacancy in Ti-rich conditions of 0.8 eV. Our formation energy of oxygen vacancy calculated by the sX functional is larger than that calculated by GGA + U. They also calculated the Ti interstitial, and found the formation of the neutral interstitial to be 0.26 eV in Ti-rich conditions. The U parameters were fitted to give a deep state for the $0/2+$ transition level of the O vacancy, and it is indeed found to be deep.

Mattioli *et al.*[36] also calculated the O vacancy and Ti interstitial, giving formation energies, and using the GGA + U method. They gave two sets of results, one with U only on Ti $3d$ orbitals, and one for U on both Ti $3d$ and O $2p$. The latter was used to open up the band gap, but it still only reached 2.7 eV in rutile. They found lower formation energies for the O vacancy than Morgan but higher formation energies for the Ti interstitial.

Many of the defect calculations using GGA + U focused on the charge localization issue, as GGA + U is useful for large supercells that are needed to study surface defects for surface chemistry and catalysis problems.

Figure 11 compares the formation energy of the neutral O vacancy and neutral Ti interstitial defects in sX as a function of the O chemical potential. This shows that the O vacancy is the more stable defect for higher O-rich μ_O values but that the Ti interstitial becomes the more stable defect below $\mu_O = -2.8$ eV. This does rationalize the various arguments in favor of the O vacancy being dominant on TiO_2 surfaces,[9–13,18,19] while the Ti interstitial can contribute in the Ti-rich situation. Note that our crossover μ_O value differs from that of Morgan and Watson[33] because their GGA + U method gave poorer

TABLE II. Comparison of formation energies and transition levels for O vacancy and Ti interstitial, calculated by different methods, this work and Refs. 33, 36, and 51.

	$V_O{}^0$ formation energy (eV), O-poor condition	O vacancy $0/+2$ transition level (eV), above VB	$Ti_i{}^0$ formation energy (eV), O-poor condition	Ti_i $0/+4$ transition (eV) above VB
sX, this work	1.9	2.3	0.3	2.85
HSE[51]	1.8	3.1		
GGA + U[33]	0.8	2.3	0.26	2.7
GGA + U[36]	0	2.0	1.2	2.5

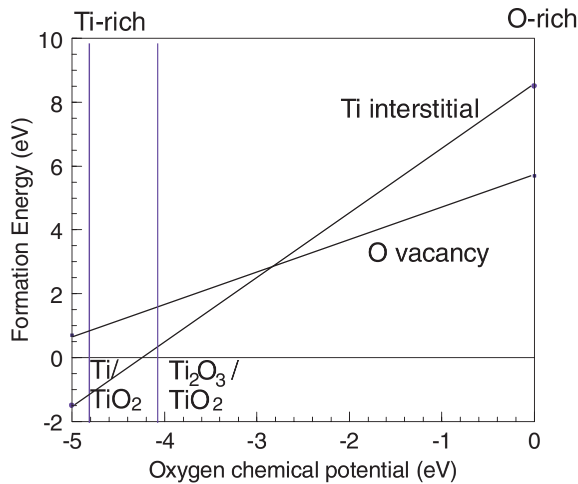

FIG. 11. (Color online) Formation of energy of the neutral O vacancy and neutral Ti interstitial as a function of O chemical potential, showing the crossover of defect stability at chemical potentials below -2.8 eV.

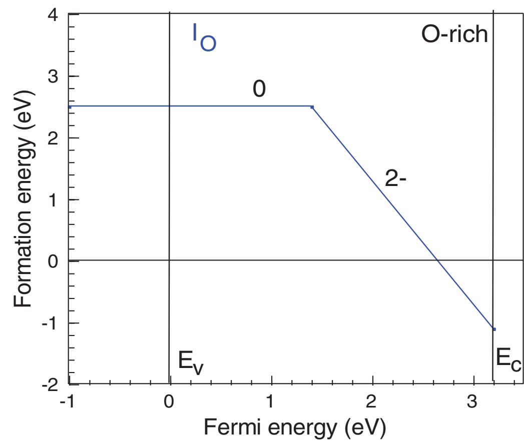

FIG. 12. (Color online) Formation energy vs. Fermi energy of the oxygen interstitial defect in rutile TiO_2.

values for the heat of formation of TiO_2. This is also the case for the results of Mattioli *et al.*[36] Interestingly, for the O-poor condition, the formation energy of $Ti_i{}^0$ calculated by sX is 0.35 eV, less than for the O vacancy. Just below this, the Ti_2O_3 phase becomes the more stable.

E. Oyxgen interstitial

The oxygen interstitial is the principle oxygen-excess defect. Its neutral configuration is the most stable across most of the range of Fermi energies (Fig. 12). In this configuration, the interstitial O forms a dumbell O-O bonded ion with a lattice oxygen. In the -1 configuration it also forms a dumbell, but with a longer O-O bond, while in its -2 structure the interstitial forms a separate ion. The O interstitial is able to show all its charge states in our sX calculation. Morgan and Watson[33] also studied the O interstitial, but because the GGA + U method is not able to open up the TiO_2 gap correctly, being a closed shell system, they could not access the negative charge states so easily. The O interstitial here behaves similarly to that in HfO_2.[73]

IV. CONCLUSIONS

We have calculated the oxygen vacancy and titanium interstitial in rutile TiO_2 using the sX hybrid functional. The sX method gives a band gap of 3.1 eV, close to the experimental value. The oxygen vacancy gives rise to localized defect states in the band gap, 0.7 eV below the conduction band, and their charge density are strongly localized on two of the three adjacent Ti atoms. The Ti interstitial also gives localized gap states, at 0.7–1.3 eV below the conduction band edge with their charge density localized on the interstitial and the adjacent Ti atoms. The formation energies of the neutral Ti interstitial falls below that of the oxygen vacancy in the Ti-rich limit. In O-rich limit, the oxygen vacancy is easier to form compared to the Ti interstitial. The results for vacancy formation energy are similar to those found by HSE, but we find a deep 0/2+ level, consistent with ESR and EELS experiments, whereas HSE finds a shallow level.

*jr214@cam.ac.uk

[1] U. Diebold, Surf. Sci. Rep. **48**, 53 (2003).
[2] T. L. Thompson and J. R. Yates, Chem. Rev. **106**, 4428 (2006).
[3] A. Fujishima, X. Zhang, and D. A. Tryk, Surf. Sci. Rep. **63**, 515 (2008).
[4] M. Gratzel, Nature (London) **414**, 338 (2001).
[5] J. Robertson, Rep. Prog. Phys. **69**, 327 (2006).
[6] R. Waser, R. Dittmann, G. Staikov, and K. Szot, Adv. Mater. **21**, 2632 (2009).
[7] S. G. Park, B. Magyari-Kope, and Y. Nishi, Phys. Rev. B **82**, 115109 (2010).
[8] V. E. Henrich, G. Dresselhaus, and H. J. Zeiger, Phys. Rev. Lett. **36**, 1335 (1976).
[9] R. L. Kurtz, R. Stockbauer, T. E. Madey, E. Roman, and J. L. Desegovia, Surf. Sci. **218**, 178 (1989).
[10] M. Nolan, S. D. Elliott, J. S. Mulley, R. A. Bennett, M. Basham, and P. Mulheran, Phys. Rev. B **77**, 235424 (2008).
[11] W. Gopel, J. A. Anderson, D. Frankel, M. Jaehnig, K. Phillips, J. A. Schafer, and G. Rocker, Surf. Sci. **139**, 333 (1984).
[12] M. A. Henderson, W. S. Epling, C. H. F. Peden, and C. L. Perkins, J. Phys. Chem. B **107**, 534 (2003).
[13] Z. M. Zhang, S. P. Jeng, and V. E. Henrich, Phys. Rev. B **43**, 12004 (1991).
[14] S. Yang, L. E. Halliburton, A. Manivannan, P. H. Bunton, D. B. Baker, M. Klemm, S. Horn, and A. Fujishima, Appl. Phys. Lett. **94**, 162114 (2009).
[15] S. Wendt, P. T. Springer, E. Lira, G. Madsen, Z. Li, J. O. Hansen, J. Matthiesen, B. Hammer, and F. Besenbacher, Science **320**, 1755 (2008).

[16]S. A. Chambers, S. H. Cheung, V. Shutthanandan, S. Thevuthasan, M. K. Bowman, and A. G. Joly, Chem. Phys. Lett. **339**, 27 (2007).
[17]M. Bowker and R. A. Bennett, J. Phys.: Condens. Matter **21**, 434224 (2009).
[18]K. Mitsuhara, H. Okumura, A. Visikovskiy, M. Takizawa, and Y. Kido, J. Chem. Phys. **136**, 124707 (2012).
[19]C. M. Yim, C. L. Pang, and G. Thornton, Phys. Rev. Lett. **104**, 036806 (2010).
[20]P. Kruger, J. Jupille, S. Bourgeois, B. Domenichini, A. Verdini, L. Floreano, and A. Morgante, Phys. Rev. Lett. **108**, 126803 (2012).
[21]M. Ramamoorthy, R. D. King-Smith, and D. Vanderbilt, Phys. Rev. B **49**, 7709 (1994).
[22]E. Cho, S. Han, H. S. Ahn, K. R. Lee, S. K. Kim, and C. S. Hwang, Phys. Rev. B **73**, 193202 (2006).
[23]J. M. Sullivan and S. C. Erwin, Phys. Rev. B **67**, 144415 (2003).
[24]S Na-Phattalung, M. F. Smith, K. Kim, M. H. Du, S. H. Wei, S. B. Zhang, and S. Limpijumnong, Phys. Rev. B **73**, 125205 (2006).
[25]H. Peng, Phys. Lett. A **372**, 1527 (2008)
[26]P. Mori-Sanchez, A. J. Cohen, and W. T. Yang, Phys. Rev. Lett. **100**, 146401 (2008).
[27]G. Pacchioini, J. Chem. Phys. **128**, 182505 (2008).
[28]M. V. Ganduglia-Pirovano, A. Hofmann, and J. Sauer, Surf. Sci. Rep. **62**, 219 (2007).
[29]S. L. Dudarev, G. A. Botton, S. Y. Savrasov, C. J. Humphreys, and A. P. Sutton, Phys. Rev. B **57**, 1505 (1998).
[30]B. J. Morgan and G. W. Watson, Surf. Sci. **601**, 5034 (2007).
[31]B. J. Morgan and G. W. Watson, Phys. Rev. B **80**, 233102 (2009) .
[32]B. J. Morgan and G. W. Watson, J. Phys. Chem. C **113**, 7322 (2009).
[33]B. J. Morgan and G. W. Watson, J. Phys. Chem. C **114**, 2321 (2009).
[34]J. Osorio-Guillen, S. Lany, and A. Zunger, Phys. Rev. Lett. **100**, 036601 (2008).
[35]E. Finazzi, C. Di Valentin, G. Pacchioni, and A. Selloni, J. Chem. Phys. **129**, 154113 (2008).
[36]G. Mattioli, P. Alippi, F. Filippone, R. Caminiti, and A. A. Bonapasta, J. Phys. Chem. C **114**, 21694 (2010).
[37]G. Mattioli, F. Filippone, P. Alippi, and A. Amore Bonapasta, Phys. Rev. B **78**, 241201 (2008).
[38]J. Stausholm-Moller, H. H. Kristoffersen, B. Hinnemann, G. K. H. Madsen, and B. Hammer, J. Chem. Phys. **133**, 144708 (2010).
[39]S. Chretien and H. Metiu, J. Phys. Chem. C **115**, 4696 (2011).
[40]C. J. Calzado, N. C. Hernandez, and J. F. Sanz, Phys. Rev. B **77**, 045118 (2008).
[41]A. C. Papageorgiou, S. Beglitis, C. L. Pang, G. Teobaldi, G. Cabaith, Q. Chen, A. J. Fisher, W. A. Hofer, and G. Thornton, PNAS **107**, 2391 (2010).
[42]P. M. Kowalski, M. F. Camellone, N. N. Nair, B. Meyer, and D. Marx, Phys. Rev. Lett. **105**, 146405 (2010).
[43]N. A. Deskins, R. Rousseau, and M. Dupuis, J. Phys. Chem. C **115**, 7562 (2011).
[44]D. C. Cronemeyer, Phys. Rev. **87**, 876 (1952); A. Amtout and R. Leonelli, Phys. Rev. B **51**, 6842 (1995).
[45]S. Lany and A. Zunger, Phys. Rev. B **80**, 085202 (2009).
[46]C. DiValentin, G. Pacchioni, and A. Selloni, Phys. Rev. Lett. **97**, 166803 (2006).
[47]C. DiValentin, G. Pacchioni, and A. Selloni, J. Phys. Chem. C **113**, 20543 (2009).
[48]C. DiValentin and A. Selloni, J. Phys. Chem. Lett. **2**, 2233 (2011).
[49]J. Muscat, A. Wader, and N. M. Harrison, Chem. Phys. Lett. **342**, 397 (2001).
[50]Y. F. Zhang, W. Lin, Y. Li, K. N. Ding, and J. Q. Li, J. Phys. Chem. B **109**, 19270 (2005).
[51]A. Janotti, J. B. Varley, P. Rinke, N. Umezawa, G. Kresse, and C. G. Van de Walle, Phys. Rev. B **81**, 085212 (2010).
[52]P. Deak, B. Aradi, and T. Frauenheim, Phys. Rev. B **83**, 155207 (2011).
[53]J. Heyd, G. E. Scuseria, and M. Ernzerhof, J. Chem. Phys. **118**, 8207 (2003).
[54]J. Heyd, G. E. Scuseria, and M. Ernzerhof, J. Chem. Phys. **124**, 219906 (2006).
[55]D. M. Bylander and L. Kleinman, Phys. Rev. B **41**, 7868 (1990).
[56]A. Seidl, A. Gorling, P. Vogl, J. A. Majewski, and M. Levy, Phys. Rev. B **53**, 3764 (1996).
[57]S. J. Clark and J. Robertson, Phys. Rev. B **82**, 085208 (2010).
[58]K. Xiong, J. Robertson, M. C. Gibson, and S. J. Clark, Appl. Phys. Lett. **87**, 183505 (2005).
[59]R. Gillen and J. Robertson, Phys. Rev. B **85**, 014117 (2012) .
[60]S. J. Clark, J. Robertson, S. Lany, and A. Zunger, Phys. Rev. B **81**, 115311 (2010).
[61]Y. Guo, S. J. Clark, and J. Robertson, J. Phys.: Condens. Matter **24**, 325504 (2012).
[62]R. Gillen and J. Robertson (unpublished).
[63]S. J. Clark, M. D. Segall, C. J. Pickard, P. J. Hasnip, M. J. Probert, K. Refson, and M. C. Payne, Z. Kristallogr. **220**, 567 (2005).
[64]S. Lany and A. Zunger, Phys. Rev. B **78**, 235104 (2008).
[65]L. D. Finkelstein *et al.*, Phys. Rev. B **60**, 2212 (1999).
[66]O. Kubaschewski and C. B. Alcock, *Metallurgical Thermochemistry* (Elsevier, New York, 1979).
[67]S. J. Clark, J. Robertson, S. Lany, and A. Zunger, Phys. Rev. B **81**, 115311 (2010).
[68]OPIUM pseudopotential package, http://opium.sourceforge.net.
[69]E. Finazzi, C. Di Valentin, and G. Pacchioni, J. Phys. Chem. C **113**, 3382 (2009).
[70]P. F. Chester, J. Appl. Phys. **32**, 2233 (1961).
[71]P. W. Peacock and J. Robertson, Appl. Phys. Lett. **83**, 2025 (2003).
[72]D. A. Panayotov and J. T. Yates, Chem. Phys. Lett. **436**, 204 (2007).
[73]S. J. Clark, L. Lin, and J. Robertson, Microelectron. Eng. **88**, 1454 (2011).